RTD-Lite: Scalable Topological Analysis for Comparing Weighted Graphs in Learning Tasks

Eduard Tulchinskii
Skoltech, AI Foundation and Algorithm Lab

Daria Voronkova
Skoltech, AIRI

Ilya Trofimov
Skoltech

Evgeny Burnaev
Skoltech, AIRI

Serguei Barannikov
Skoltech, CNRS

Abstract

Topological methods for comparing weighted graphs are valuable in various learning tasks but often suffer from computational inefficiency on large datasets. We introduce RTD-Lite, a scalable algorithm that efficiently compares topological features, specifically connectivity or cluster structures at arbitrary scales, of two weighted graphs with one-to-one correspondence between vertices. By leveraging minimal spanning trees in auxiliary graphs, RTD-Lite captures topological discrepancies with $O(n^2)$ time and memory complexity. This efficiency enables its application in tasks like dimensionality reduction and neural network training. Experiments on synthetic and real-world datasets demonstrate that RTD-Lite effectively identifies topological differences while significantly reducing computation time compared to existing methods. Moreover, integrating RTD-Lite into neural network training as a loss function component enhances the preservation of topological structures in learned representations. Our code is publicly available at `https://github.com/ArGintum/RTD-Lite`.

1 INTRODUCTION

The analysis and comparison of weighted graphs are fundamental tasks in numerous fields such as machine learning, network science, and computational biology. Graph representations are ubiquitous for modeling complex systems, where nodes represent entities and edges represent relationships or interactions with associated weights. In learning tasks, comparing the structural properties of these graphs can reveal significant insights into the underlying data, such as identifying community structures, detecting anomalies, or understanding the evolution of networks over time.

Topological data analysis (TDA) provides robust tools like persistence barcodes to capture multi-scale topological features of data (Barannikov, 1994; Zomorodian, 2001; Chazal and Michel, 2021), which are valuable for comparing complex structures like weighted graphs. The Representation Topology Divergence (RTD) Barannikov et al. (2021) is one such method that quantifies the topological dissimilarity between two weighted graphs based on comparative cross-barcodes. While RTD provides a rigorous measure of topological differences, it may become computationally intensive for large-scale graphs due to the high complexity of computing persistence barcodes.

In practical applications involving large datasets, there is a critical need for methods that can efficiently compare the topological features of weighted graphs without compromising on the quality of the insights gained. Existing approaches either fail to capture essential topological characteristics at multiple scales or do not scale well with the size of the data, limiting their applicability in real-world scenarios.

In this paper, we introduce **RTD-Lite**, a scalable algorithm designed to efficiently compare the topological features of two weighted graphs, focusing particularly on their cluster structures. RTD-Lite leverages the concept of minimal spanning trees (MSTs) within auxiliary graphs constructed from the input graphs to capture topological discrepancies. By avoiding the computational overhead associated with calculating the full persistent homology, RTD-Lite achieves an $\mathcal{O}(n^2)$

Proceedings of the 28th International Conference on Artificial Intelligence and Statistics (AISTATS) 2025, Mai Khao, Thailand. PMLR: Volume 258.

time and memory complexity, where n is the number of vertices in the graphs.

Key contributions of our work include:

- We propose RTD-Lite as an efficient method to compute a large subset of the RTD features that focuses on zero-dimensional homology (connected components), which is computationally less intensive yet captures essential topological differences between two graphs.
- We provide a detailed computational complexity analysis of RTD-Lite, demonstrating its scalability and efficiency compared to existing methods.
- We show how RTD-Lite can be integrated into neural network training as a component of the loss function, promoting the preservation of topological structures in learned representations.
- Through extensive experiments on both synthetic and real-world datasets, we demonstrate that RTD-Lite effectively identifies topological differences between graphs. We compare its performance with existing methods, highlighting significant reductions in computation time without sacrificing accuracy.
- We explore various applications of RTD-Lite, including dimensionality reduction and analysis of neural network representations, showcasing its practical utility in large-scale learning tasks.

By addressing the computational challenges associated with topological graph comparison, RTD-Lite opens new avenues for efficiently analyzing large-scale graphs in various learning tasks. We believe that our contributions will significantly benefit researchers and practitioners working with complex networked data.

2 RELATED WORK

Comparing weighted graphs is fundamental in domains like machine learning, computational biology and network science. Traditional methods such as the graph edit distance measure the minimal transformations needed to convert one graph into another (Sanfeliu and Fu, 1983), but are NP-hard and impractical for large graphs, often focusing on local differences. Graph kernels, including the Weisfeiler-Lehman graph kernel (Shervashidze et al., 2011) and the shortest-path kernel (Borgwardt and Kriegel, 2005), provide scalable comparisons by embedding graphs into feature spaces, capturing structural properties more efficiently (Vishwanathan et al., 2010). However, they may struggle with very large graphs and may not capture multi-scale topological features.

Representation Topology Divergence (RTD), introduced in Barannikov et al. (2021), measures topological dissimilarities between two weighted graphs with one-to-one correspondence between vertices, based on comparative persistence barcodes. While RTD provides rigorous insights, its computational cost can be relatively high, especially for large graphs.

Clustering with minimum spanning trees (MSTs) has been explored by Zahn (1971), who identified clusters by removing large-weight edges from an MST. Xu et al. (1990) later enhanced this approach with a fast parallel algorithm, improving scalability for large datasets.

Recent advances have integrated TDA into graph neural networks (GNNs) to enhance graph similarity learning and representation Chen et al. (2021); Wen et al. (2024). New methods also incorporate TDA into community detection in dynamic networks, improving the consistency of cluster structures over time (Kong et al., 2024). Another direction employs merge trees alongside neural networks to enable topological comparisons of large-scale graphs (Qin et al., 2024).

Luo et al. (2021) introduced a topology-preserving dimensionality reduction method utilizing a graph autoencoder, while Moor et al. (2020); Trofimov et al. (2023) proposed incorporating additional losses to the autoencoder to maintain the topological structures of the input space in latent representations. Kim et al. (2020) proposed a differentiable topological layer for general deep learning models based on persistence landscapes. An approach for the differentiation of persistent homology-based functions was introduced by Carrière et al. (2021), and Leygonie et al. (2021) established differentiability for maps involving persistence barcodes.

3 DEFINITION AND TWO ALGORITHMS

Let A and B be two connected, undirected, weighted graphs on n vertices, with a bijection between their vertex sets (so vertex i in A corresponds to vertex i in B). We assume that the edge weights in both graphs are similarly scaled by aligning their 0.9-quantiles. For an edge e in A, let a_e denote its weight and b_e the weight of the corresponding edge in B (or plus infinity if the edge is absent). Denote by C the auxiliary graph with the same set of vertices and with weights $c_e = \min(a_e, b_e)$. Everywhere in this work when we talk about the *auxiliary graph* we understand graph C. Thus, the set of edges of C is the union of edge sets of A and B with the edge weight equal to the

minimum of the weights of the corresponding edges in A and B.

We propose a method to quantify the discrepancy between multi-scale cluster structures of two graphs, that does it in a similar fashion to RTD but without the necessity to perform persistence barcodes computation. It calculates the set of intervals (barcode) that approximates a R-Cross-Barcode$_1(A, B)$. We call it "RTD-Lite barcode" and denote it as *RTD-L-barcode*(A, B); we denote sum of its intervals lengths as RTDL(A, B).

RTD-L-barcode(A, B) is the collection of intervals $[c_e, a_{t(e)}]$, representing misalignments in multiscale cluster structure of the two weighted graphs. Here, c_x is the level at which a pair of clusters in C merges into one (i.e. the weight of an edge e from minimal spanning tree of C). Denote those two clusters (as sets of vertices) as C_1 and C_2, then the end of the interval ($a_{t(e)}$) will be the minimal level at which some of the vertices from both C_1 and C_2 belong to the same cluster in A (i.e., in A there is a path between a vertex from C_1 and a vertex from C_2 such that its maximal edge $t(e)$ has weight of $a_{t(e)}$, and there are no paths with lesser maximal weight edges). Notation $t(e)$ is used to highlight that this 'closing' edge depends on edge e.

For each edge from minimal spanning tree of C, *RTD-L-barcode*(A, B) contains exactly one interval, $n-1$ in total, some of them may have zero length and are typically discarded. Figure 2 presents a direct comparison of RTD-Lite- and R-Cross-Barcodes for a pair of point clouds with A containing one cluster and B containing three clusters shown on figure 7.

We develop two algorithms to compute RTD-Lite metric. First of them, Algorithm 1, is the direct implementation of the described procedure. However, often in practical applications instead of the full barcode only the sum of its intervals length is needed. In this case, a faster algorithm can be devised (Algorithm 2). It has better computational time asymptotic but it doesn't reconstruct the intervals, only yields the sum of their lengths. Below, we discuss both algorithms.

3.1 Direct algorithm

To compute *RTD-L-barcode*(A, B) according to the definition, we implement the following procedure (Algorithm 1). First, we normalize the weight matrices of both graphs and construct graph C as edge-wise minimum. We build minimal spanning trees (MSTs) of A and C as two lists of edges sorted by ascension of their weights. After that, we iterate over the edges from the MST of graph C and for each edge e (of weight c_e) consider a sub-forest containing all previous edges from the MST; then we run over edges from MST of graph A and add them one by one to that sub-forest until there appears a path between ends of edge e. Finally, list of intervals $[c_e; a_{t(e)}]$ one for each e from MST of graph C is outputed as *RTD-L-barcode*(A, B).

Algorithm 1 Computation of RTD-Lite Barcode

Input: M_A, M_B – weights matrices of graphs A and B respectively
Require: $MST(\cdot)$ — function computing Minimal Spanning Tree of a weighted graph, returns list of edges
Sort$(\cdot)$ – a function sorting list of edges by their weights
Output: Multiset of pairs (intervals constructing *RTD-L-barcode*(A, B))

```
procedure RTD-L-Barcode(A, B)
    M_A, M_B ← M_A, M_B divided by their 0.9 quantiles
    M_C ← element-wise minimum of M_A and M_B
    T_A, T_C ← MST(A), MST(G_C)
    T_A, T_C ← Sort(T_A), Sort(T_C)
    RTDL_barcode ← [ ]
    SubTree ← empty graph
    for each e ∈ T_C do
        v_1, v_2 ← vertices of e
        TemporaryGraph ← SubTree
        i ← 0
        repeat
            ẽ_i ← edge #i from T_A
            Add ẽ_i to TemporaryGraph
            i ← i + 1
        until v_1 and v_2 are connected in TemporaryGraph
        Add (e; ẽ_{i−1}) to RTDL_barcode
        Add e to SubTree
    end for
    return: RTDL_barcode
end procedure
```

Proposition 1. Intervals $[c_e; a_{t(e)}]$ obtained per procedure above are valid (i.e., $c_e \leq a_{t(e)}$).

Proof: Suppose the opposite, and $\exists e : c_e > a_{t(e)}$. This means there exists a path between ends of e made from edges $e_1, \ldots, e_l$ from C with weights $\leq c_e$ and edges $e_{l+1}, \ldots, e_k$ from A with weights $\leq a_{t(e)}$ and the largest of them is $t(e)$ with weight of $a_{t(e)}$. $\forall i \in \overline{l+1, \ldots k} : a_{e_i} \geq c_{e_i}$. Therefore, there is a path in C between ends of e made of edges with weights $\leq a_{t(e)} < c_e$; this contradicts the Cycle Property of MST. □

In our experiments, we operate on full or nearly full graphs thus we implement Prim's algorithm for MST computation. We use *Disjoint Set Union (DSU)* to store sub-forests appear while iterating over edges

from MST of C. Since DSU does not support erasing of edges (only addition), we make a copy of it before temporarily adding edges from MST of graph A.

Computational Complexity. The time complexity of weight normalization, and building of graph C is $O(n^2)$. MST construction via Prim's algorithm takes $O(n^2)$, and sorting edges of MST takes $O(n \log n)$ operations. At each iteration of cycle over edges from MST of C we add previous edge to DSU, make a copy of DSU structure (it has $O(n)$ size, therefore $O(n)$ operations) and add to it up to $n-1$ edges from MST of graph A. Later takes $O(n\alpha(n))$ operations where $\alpha(\cdot)$ is the inverse Ackermann function. There are $n-1$ iterations in this cycle, thus, total time complexity of this algorithm is $O(n^2) + O(n \log n) + (n-1)O(n) + (n-1)O(n\alpha(n)) = O(n^2\alpha(n))$.

This algorithm requires $O(n^2)$ additional memory: $O(n^2)$ needed to store graph C weight matrix. Each of the DSU copies requires $O(n)$ memory, but only two of them are needed to be stored at the same time; other steps require no more than linear amount of memory.

3.2 Simplified computation

To compute only RTDL(A, B) – the sum of intervals from the barcode – a simpler algorithm can be used. First, we apply the same preprocessing steps as in previous algorithm: weights normalization and construction of graph C. Then we construct MST's for graphs A and C and compute sum of edge weights in them — s_A and s_C respectively. The required RTDL(A, B) is $s_A - s_C$.

Algorithm 2 RTD-Lite returning only sum of intervals lengths

Input: M_A, M_B – weight matrices of graphs A and B respectively
Require: $MST(\cdot)$ — function computing Minimal Spanning Tree of a weighted graph, returns list of edges
Output: One real number – value of RTDL(A, B)
procedure RTD-LiteSumOnly(A, B)
$M_A, M_B \leftarrow M_A, M_B$ divided by their 0.9 quantiles
$M_C \leftarrow$ element-wise minimum of M_A and M_B
$T_A, T_C \leftarrow MST(A), MST(C)$
$s_A \leftarrow \sum_{e \in T_A} w_e$
$s_C \leftarrow \sum_{e \in T_C} w_e$
return: $s_A - s_C$
end procedure

Proposition 2. Algorithm 2 is correct; i.e., its result is equal to the sum of lengths of intervals yielded by Algorithm 1 for the same two graphs.

Proof: Sum of lengths of intervals in RTD-Lite barcode yielded by Algorithm 1 is equal to $\sum_{e \in MST(C)} \left(a_{t(e)} - c_e\right) = \sum_{e \in MST(C)} a_{t(e)} - \sum_{e \in MST(C)} c_e = \sum_{e \in MST(C)} a_{t(e)} - s_C$ We need only to show that $s_A = \sum_{e \in MST(A)} a_e = \sum_{e \in MST(C)} a_{t(e)}$. We will do it by proving that each edge from MST of graph A can be $t(e)$ for no more than one $e \in \text{MST}(C)$; bijection between set of all $t(e)$ and MST(A) will follow from them having the same size.

Suppose the opposite: there are two distinct edges from MST(C): (u_1, v_1) and (u_2, v_2) such that $t((u_1, v_1)) = t((u_2, v_2)) = (u^0, v^0)$. Let $\prec_A, \prec_C$ be strict orders in which edges are listed after being sorted in Algorithm 1, and let $(u_1, v_1) \prec_C (u_2, v_2)$. Here, as the size of a path we understand the weight of its largest edge. By its choice, $t((u_1, v_1))$ is the largest edge on the smallest path between $u_1$andv_1 made from edges of MST(A) and MST(C) excluding (u_1, v_1). That means, there exist two paths: one from u_1 to u^0 and one from v_1 to v^0 such that every edge on them is either $\prec_A (u^0, v^0)$ or $\prec_C (u_1, v_1) \prec_C (u_2, v_2)$ (depending from which MST they came). Similarly, from choice of $t((u_2, v_2))$ follows presence of paths between u_2 and u^0 and between v_2 and v^0 such that every edge on them is either $\prec_A (u^0, v^0)$ or $\prec_C (u_2, v_2)$.

Thus, there is a path between u_2 and u_1 ($u_2 \to u^0 \to u_1$) such that every edge on them is either $\prec_A (u^0, v^0)$ or $\prec_C (u_2, v_2)$ and a similar path between v_2 and v_1. Since $\prec_C (u_1, v_1) \prec_C (u_2, v_2)$, there is a path between u_2 and v_2 with the same properties. At least one edge on that path belongs to MST(A), otherwise together with (u_2, v_2) it will constitute a cycle in MST of graph C. That edge is $\prec_A (u^0, v^0)$ but this contradicts the choice of (u^0, v^0) for $t((u_2, v_2))$ in Algorithm 1 as the smallest edge with such property.

Therefore, each edge from MST(A) can correspond (in terms of $t(e)$) to no more than one $e \in \text{MST}(A)$. □

Computational Complexity. The time complexity of auxiliary steps (weight normalization, and construction of graph C) is $O(n^2)$, and Prim's algorithm for MST computation takes $O(n^2)$; total – $O(n^2)$. Algorithm requires $O(n^2)$ memory – to store graph C.

3.3 Application to comparison of neural representations

RTD-Lite can be used to compare two point clouds $P, \tilde{P}$, of the same size n with one-to-one correspondence. In this case, to estimate the discrepancy, we consider two complete graphs A, B having n vertices with edge weights equal to pairwise distances of $P, \tilde{P}$ respectively. In particular, $P, \tilde{P}$ can be two neural representations of same objects. We estimate the topo-

logical discrepancy between representations $P, \tilde{P}$ as $\mathrm{RTDL}(A, B)$.

3.4 Gradient Optimization

Ends of intervals constituting RTD-Lite barcode are either edge weights from one of the graphs or minimums of weights of two corresponding edges. In both cases, they are (sub-)differentiable by edge weights; therefore for a differentiable function of RTD-Lite barcode (e.g. sum of bars lengths) its (sub-)gradient at edge weights in A and B can be computed. Often edge weights are distances within a point cloud and the (sub-)gradients can be further propagated via the chain rule.

4 RTD-LITE COMPARES TWO GRAPHS MULTI-SCALE CLUSTERS

In this section, we compare the connected components of two graphs across various scales. For any threshold value α, we consider the sub-graphs $A^{\leq\alpha}$ and $C^{\leq\alpha}$, which include all edges with weights less than or equal to α in graphs A and C, respectively. Notice that the set of edges in $C^{\leq\alpha}$ is the union of sets of edges in $A^{\leq\alpha}$ and $B^{\leq\alpha}$

The zeroth homology group $H_0(G)$ over field k of a graph G is the vector space $k^{\#G}$ where $\#G$ is the set of connected components of G. The inclusion of $A^{\leq\alpha}$ into $C^{\leq\alpha}$ induces a linear map between their homology groups, denoted as

$$r_{0,\alpha} : H_0(A^{\leq\alpha}) \to H_0(C^{\leq\alpha}).$$

This map sends a connected components of $A^{\leq\alpha}$ to the corresponding component in $C^{\leq\alpha}$. We have the following exact sequence of linear maps of homology groups:

$$0 \to \ker(r_{0,\alpha}) \xrightarrow{\iota} H_0(A^{\leq\alpha}) \xrightarrow{r_{0,\alpha}} H_0(C^{\leq\alpha}) \to 0, \quad (1)$$

where: 0 denotes the trivial group, $\ker(r_{0,\alpha})$ is the kernel of $r_{0,\alpha}$, it is linearly generated by pairs of connected components in $A^{\leq\alpha}$ that map to the same component in $H_0(C^{\leq\alpha})$, ι is the inclusion map.

The sequence 1 is exact, meaning that the image of each map is equal to the kernel of the subsequent map. This exactness captures the precise relationship between the connected components of $A^{\leq\alpha}$ and $C^{\leq\alpha}$. The exact sequence in (1) provides critical insights into how the topology of graph A changes when combined with graph B to form graph C. Specifically: the kernel $\ker(r_{0,\alpha})$ represents connected components in $A^{\leq\alpha}$ that are not preserved in $C^{\leq\alpha}$ due to the influence of B; the map $r_{0,\alpha}$ identifies how these components merge or split when transitioning from $A^{\leq\alpha}$ to $C^{\leq\alpha}$. The definition of RTD-Lite barcode implies that the dimension of $\ker(r_{0,\alpha})$ equals the number of intervals in RTD-Lite barcode that contain α, see Appendix.

This analysis allows us to quantify the topological differences between the two graphs at different scales, which is essential for applications that require multi-scale connectivity comparisons.

5 EXPERIMENTS

5.1 Comparing point clouds and neural representations

5.1.1 Experiments with synthetic data

To illustrate the behavior of RTD-Lite for common data comparison scenarios, we perform small-scale experiments on synthetic point clouds: "Clusters" and "Rings".

"Rings" data. We compare synthetic point clouds consisting of a variable number of rings, see Figure 1, top. The initial point cloud consists of 500 points uniformly distributed over the unit circle. Then, the points are moved onto circles with radii varying from 0.5 to 1.5. Finally, we compare the point cloud having 5 rings with other ones. Figure 1, bottom, demonstrates that both RTD and RTD-Lite almost ideally reflect the change of the topological complexity while CKA fails.

"Clusters" data. The initial point cloud consists of 300 points randomly sampled from the 2-dimensional normal distribution having zero mean (Figure 7, top). Next, we split it into $2, 3, \ldots 12$ parts (clusters) and move them to the circle of radius 10. We compare the initial point cloud (having one cluster) with the split ones by calculating: RTD (Barannikov et al., 2021), RTD-Lite and CKA (Kornblith et al., 2019), see Figure 7, top. Both RTD-Lite and RTD change monotonically w.r.t. number of clusters, while CKA changes chaotically. Interestingly, RTD-Lite decreases monotonically, indicating that clusters located on the circle of radius 10 tend to create a single cluster, like the initial point cloud (the leftmost in Figure 7, top).

For additional comparisons with SVCCA (Raghu et al., 2017) and IMD (Tsitsulin et al., 2020) see Appendix D.

5.1.2 Visualization of RTD-Lite-Barcodes

RTD-Lite also creates a list of intervals which is called RTD-Lite Barcodes (see Algorithm 1) depicting a multi-scale differences in topological structures. R-Cross-Barcodes from Barannikov et al. (2021) and

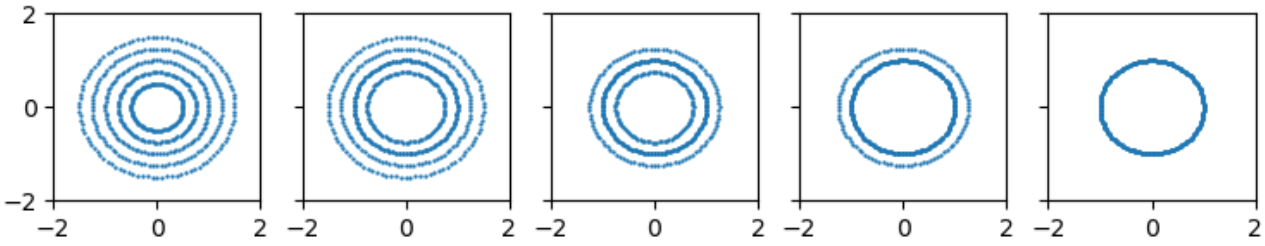

(a) Point clouds used in 'the 'rings" experiment.

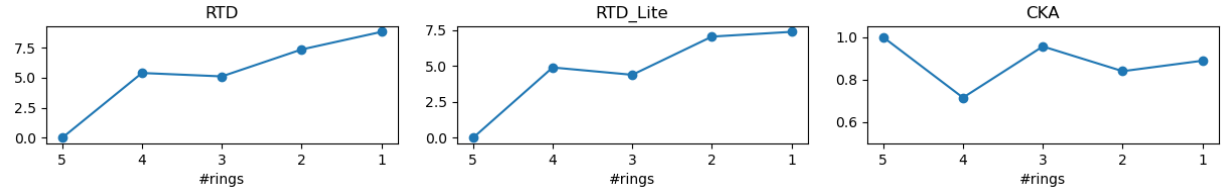

(b) Representations' comparison measures. Ideally, the measure should change monotonically with the increase of topological discrepancy.

Figure 1: RTD-Lite along with RTD perfectly detect cluster structures, while rival measures fail. Five connected components (rings) are compared with 1-5 rings.

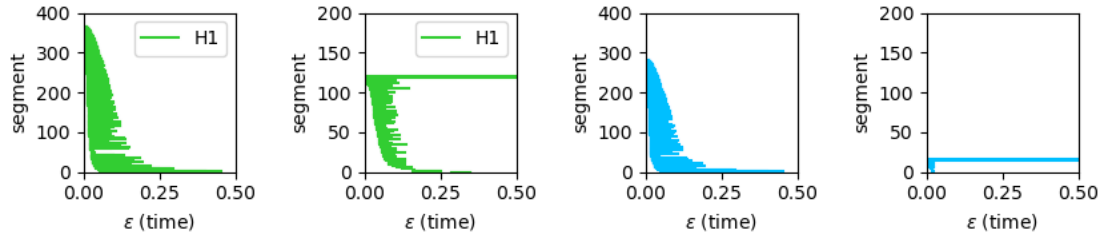

(a) R-Cross-Barc.(A, B) (b) R-Cross-Barc.(B, A) (c) RTD-L-Barc.(A, B) (d) RTD-L-Barc.(B, A)

Figure 2: Cross-Barcodes for comparison of 1 cluster (A) vs. 3 clusters (B).

RTD-Lite Barcodes are depicted in Figure 2. The barcodes have some similarities, see more examples in Appendix C.

5.1.3 Comparing representations from UMAP

In this experiment, we verify whether RTD-Lite is able to capture the growing topological dissimilarity of representation spaces of real data. For this purpose, we apply UMAP (McInnes et al., 2018), the state-of-the-art dimensionality reduction method, to get 2D representations of the MNIST dataset. In UMAP, we vary the number of neighbors in the range $(10, 20, 50, 100, 200)$, see Figure 3a. The number of neighbors in UMAP affects the topological structure: for low values, the algorithm focuses on the local structure and clusters are crisp; for high values, the algorithm pays more attention to the global structure, and clusters overlap often. Then, we perform the pairwise comparison of all the variants of 2D representations by RTD, RTD-Lite and CKA, see Figure 3. CKA reveals a chaotic pattern w.r.t. number of neighbors. In contrast, both RTD and RTD-Lite have monotonic increasing behavior which coincides with the growing dissimilarity in UMAP representations.

5.1.4 Comparing Representations of DNN layers

We evaluate the proposed RTD-Lite with sanity tests: in pairwise comparisons of layers' representations from networks trained with different initializations, the corresponding layers are expected to be the closest ones. To account for versatile structure of the underlying data, we perform this experiment for both CNN and GNN architectures.

CNN architecture. We train All-CNN networks Springenberg et al. (2014) on CIFAR-10 with 10 different seeds. Figure 4 depicts averaged comparisons of representations from all convolutional layers (after batch normalization). RTD-Lite provides an accurate estimate of the RTD behavior pattern. We also carried

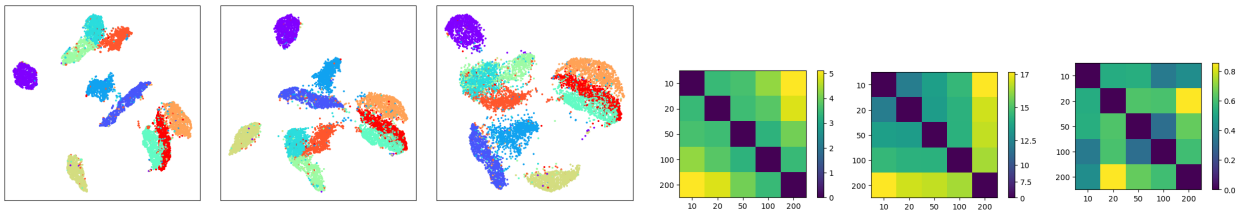

(a) 2D representations of MNIST. (b) RTD (c) RTD-Lite (d) 1-CKA

Figure 3: Comparing representations of MNIST by UMAP with varying n_neighbors. Left: representations with n_neighbors = 10, 50, 200. Right: comparison of representations by metrics.

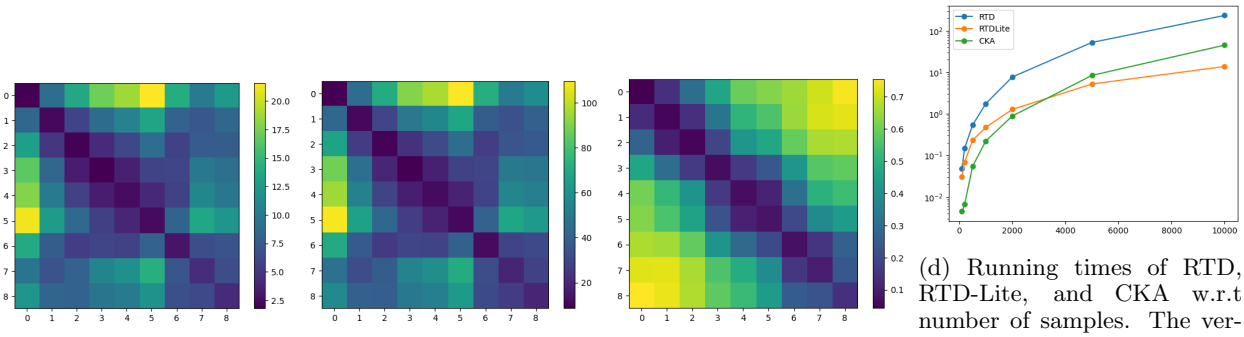

(a) RTD (b) RTD-Lite (c) 1-CKA (d) Running times of RTD, RTD-Lite, and CKA w.r.t number of samples. The vertical axis is log-scaled.

Figure 4: Comparing layers from All-CNN networks trained on CIFAR10 with different seeds.

out a classification experiment where for each layer the predicted corresponding layer was selected by metrics under analysis. The classification accuracy obtained: RTD - 98%, RTD-Lite - 98%, CKA - 96%. The calculation of RTD-Lite was ~ 6 times faster than RTD.

GNN architecture. We strictly follow the setup from Ebadulla and Singh (2024) and train four GNN architectures — GCN (Kipf and Welling, 2016), GraphSAGE (Hamilton et al., 2017), GAT (Velickovic et al., 2017) and ClusterGCN (Chiang et al., 2019) — to solve Node Classification task on the Amazon Computers dataset (Shchur et al., 2018). Figures 5a-5d demonstrates that RTD-Lite has lowest values for the corresponding layers among all pairwise comparisons for all the architectures. By comparing RTD and RTD-Lite scores in Figure 5e, we reveal that both metrics are well aligned.

5.2 Running times and computational complexity

To compare two representations of n objects having dimensionalities d_1, d_2, the methods under analysis have the following computational complexity: CKA - $O(n^3+n^2(d_1+d_2))$, RTD-Lite - $O(n^2(\alpha(n)+d_1+d_2))$. For computation of RTD, one should calculate pairwise distances having cost $O(n^2(d_1+d_2))$. However, the computation of RTD is dominated by the persistence barcode evaluation, which is at worst cubic in the number of simplices involved. The later one increases at least exponentially with n. In practice, the computation is much faster since the boundary matrix is typically sparse for real datasets.

Running times of RTD, RTD-Lite, and CKA w.r.t. number of samples n are depicted in Figure 4d. We used embeddings of CIFAR10 from a CNN for testing. RTD-Lite is significantly faster than RTD. For small n, CKA is fast probably because of a multicore implementation of matrix multiplication in `numpy`. For large n, RTD-Lite is the fastest method.

Additionally, we carried out an experiment for comparison of layers' representations for a larger data of size 50k (full CIFAR10 train dataset) corresponding to graphs having 50k vertices. Running times are the following: RTD-Lite: 3.75 minutes, RTD: out of GPU memory, CKA: 36 minutes. Standard RTD metric is not applicable for such large data, while RTD-Lite is 10 times faster than CKA.

5.3 Analysis of gradient optimization

Here we show that our method can be used not only as static metric but also as a loss function component during training of neural networks. We illustrate this on task of dimensionality reduction. Here we follow the setup proposed in Trofimov et al. (2023)

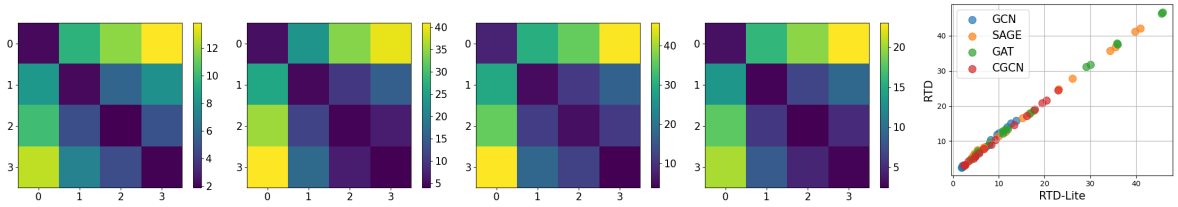

(a) GCN (b) SAGE (c) GAT (d) CGCN (e) RTD-Lite vs. RTD

Figure 5: RTD-Lite scores between layers from GNNs trained with different seeds.

and implement a deep autoencoder in which loss function has integrated component of RTD-Lite between original high-dimensional data and their low-dimensional representations. Therefore, given the data $X = \{x_i\}_{i=1}^n, x_i \in \mathrm{R}^d$ and its latent representation $Z = \{z_i\}_{i=1}^n, z_i \in \mathrm{R}^d$, the training loss function will be $\frac{1}{n}||X - X_{rec}||_2^2 + \frac{\lambda}{2n}\left(\mathrm{RTDL}(X, Z) + \mathrm{RTDL}(Z, X)\right)$, where λ is a hyperparameter. This loss is computed on mini-batches.

We compare the proposed RTD-Lite AE againts the RTD-AE Trofimov et al. (2023), as well as vanilla autoencoder (AE), and TopoAE Moor et al. (2020). Also, for reference, we provide results of applying UMAP Damrich and Hamprecht (2021) to the same data. Autoencoder models implement the same architecture and differ only in the training loss. The complete descriptions of datasets and hyperparameters used are provided in Appendix. We evaluate these methods by four metrics comparing original data and their latent representations. They are: (1) linear correlation of pairwise distances, (2) Wasserstein distance between H_0 persistence barcodes Chazal and Michel (2021), (3) Triplet distance ranking Accuracy Wang et al. (2021), and finally (4) RTD. All of these metrics are tailored at measuring how good the manifold's global structure and topology are preserved within latent representations; however, they work on different principles and capture different aspects of the matter; therefore, we report all four of them.

Synthetic data. First, we used our method at a synthetic dataset "Spheres". It consists of 10,000 points randomly sampled from surfaces of eleven 100D spheres lying in R^{101}; none of them intersect, and one contains all others inside.

Results are presented in Table 1. From it we can see that RTD-Lite autoencoder performs slightly worse than RTD-AE or TopoAE but overall is still on somewhat equal level with them. RTD-AE achieves the best quality by almost all metrics. Training of autoencoder with RTD-Lite loss, however, is much faster than of one with RTD loss and unlike later it does not require the two-stage procedure when autoencoder is trained with reconstruction loss only for first several epochs.

Table 1: Quality of data manifold global structure preservation at projection Spheres dataset.

	Quality measure			
Method	L. C.	W. D. H_0	T. A.	RTD
into 2D space				
UMAP	0.021	44.90 ± 1.8	0.54 ± 0.01	42.60 ± 1.8
AE	0.311	46.07 ± 1.5	0.41 ± 0.01	41.02 ± 1.4
TopoAE	0.495	43.92 ± 2.5	0.54 ± 0.02	39.69 ± 1.4
RTD	0.626	45.29 ± 2.2	0.68 ± 0.02	39.60 ± 1.9
RTD-L	0.570	45.72 ± 2.0	0.64 ± 0.02	40.00 ± 1.7
into 3D space				
UMAP	0.041	45.56 ± 2.2	0.54 ± 0.01	41.79 ± 2.2
AE	0.376	46.06 ± 2.3	0.41 ± 0.02	41.05 ± 2.2
TopoAE	0.622	40.41 ± 2.7	0.71 ± 0.01	34.74 ± 1.9
RTD	0.687	41.39 ± 2.3	0.74 ± 0.02	33.74 ± 1.6
RTD-L	0.615	41.76 ± 1.8	0.66 ± 0.02	35.80 ± 1.5

Table 2: Global structure preservation quality during dimensionality reduction of real-life datasets.

	Quality measure			
Method	L. C.	W. D. H_0	T. A.	RTD
F-MNIST into 16D space				
UMAP	0.602	592.0 ± 3.9	0.741 ± 0.02	12.31 ± 0.4
AE	0.879	320.5 ± 1.9	0.850 ± 0.00	5.52 ± 0.2
TopoAE	0.905	190.7 ± 1.2	0.867 ± 0.01	3.69 ± 0.2
RTD	0.960	181.2 ± 0.8	0.907 ± 0.00	3.01 ± 0.1
RTD-L	0.933	181.7 ± 1.4	0.910 ± 0.01	3.75 ± 0.2
COIL-20 into 16D space				
UMAP	0.301	274.7 ± 0.0	0.574 ± 0.01	15.99 ± 0.5
AE	0.834	183.6 ± 0.0	0.809 ± 0.01	8.35 ± 0.2
TopoAE	0.910	148.0 ± 0.0	0.822 ± 0.02	6.90 ± 0.2
RTD	0.944	88.9 ± 0.0	0.892 ± 0.01	5.78 ± 0.1
RTD-L	0.949	77.1 ± 0.0	0.898 ± 0.01	5.35 ± 0.2

Real-life datasets. We performed similar style experiments with two real-world datasets: F-MNIST (Xiao et al., 2017), and COIL-20 (Nene et al., 1996). Unlike *Spheres*, these datasets doesn't have such clear multi-dimensional internal structures and are much more noisy. These datasets have much higher number of parameters, and so for them we choose latent dimension of size 16. Table 2 presents the results. In this situation, RTD-Lite AE performs at level of RTD-AE and noticeable better than other methods.

6 CONCLUSION

Our method, RTD-Lite, streamlines topological feature computation for graphs having one-to-one correspondence between nodes by focusing on comparing multi-scales cluster structures via MSTs on auxiliary graphs, achieving $\mathcal{O}(n^2)$ complexity. This reduces the computational load significantly w.r.t standard RTD metric. RTD-Lite works well as a tool for comparing neural representations of CNNs and GNNs. Moreover, RTD-Lite integrates efficiently as a loss function in neural network training for dimensionality reduction, preserving both global and local data structures without the overhead of full persistence barcode calculations.

Acknowledgments

Research was partially supported by the funding of Skoltech Applied AI center.

References

S. Barannikov. The framed Morse complex and its invariants. *Advances in Soviet Mathematics*, 21:93–116, 1994.

S. Barannikov, I. Trofimov, N. Balabin, and E. Burnaev. Representation topology divergence: A method for comparing neural network representations. In *Proceedings of the 39th International Conference on Machine Learning*, volume 162, pages 1607–1626, 2021.

K. M. Borgwardt and H.-P. Kriegel. Shortest-path kernels on graphs. In *Proceedings of the 5th IEEE International Conference on Data Mining (ICDM)*, pages 74–81. IEEE, 2005.

M. Carrière, M. Cuturi, and S. Oudot. Optimizing persistent homology based functions. *International Conference on Machine Learning (ICML)*, pages 1294–1303, 2021.

B. P. Chamberlain, J. Rowbottom, M. I. Gorinova, S. D. Webb, E. Rossi, and M. M. Bronstein. GRAND: Graph neural diffusion. In *The Symbiosis of Deep Learning and Differential Equations*, 2021. URL `https://openreview.net/forum?id=_1fu_cjsaRE`.

F. Chazal and B. Michel. An introduction to topological data analysis: fundamental and practical aspects for data scientists. *Frontiers in artificial intelligence*, 4:667963, 2021.

Y. Chen, B. Coskunuzer, and Y. Gel. Topological relational learning on graphs. *Advances in neural information processing systems*, 34:27029–27042, 2021.

W.-L. Chiang, X. Liu, S. Si, Y. Li, S. Bengio, and C.-J. Hsieh. Cluster-gcn: An efficient algorithm for training deep and large graph convolutional networks. In *Proceedings of the 25th ACM SIGKDD international conference on knowledge discovery & data mining*, pages 257–266, 2019.

S. Damrich and F. A. Hamprecht. On umap's true loss function. *Advances in Neural Information Processing Systems*, 34:5798–5809, 2021.

D. Ebadulla and A. Singh. Normalized space alignment: A versatile metric for representation space discrepancy minimization, 2024. URL `https://openreview.net/forum?id=5HGPR6fg2S`.

N. Entezari, S. A. Al-Sayouri, A. Darvishzadeh, and E. E. Papalexakis. All you need is low (rank): Defending against adversarial attacks on graphs. In *Proceedings of the 13th International Conference on Web Search and Data Mining*, WSDM '20, page 169–177, New York, NY, USA, 2020. Association for Computing Machinery. ISBN 9781450368223. doi: 10.1145/3336191.3371789. URL `https://doi.org/10.1145/3336191.3371789`.

W. Hamilton, Z. Ying, and J. Leskovec. Inductive representation learning on large graphs. *Advances in neural information processing systems*, 30, 2017.

W. Jin, Y. Ma, X. Liu, X. Tang, S. Wang, and J. Tang. Graph structure learning for robust graph neural networks. In *Proceedings of the 26th ACM SIGKDD International Conference on Knowledge Discovery & Data Mining*, KDD '20, page 66–74, New York, NY, USA, 2020. Association for Computing Machinery. ISBN 9781450379984. doi: 10.1145/3394486.3403049. URL `https://doi.org/10.1145/3394486.3403049`.

H. Kim, J. Lee, U. Kang, and J. Choo. Pl-lay: Efficient layer-wise topological regularization. *Proceedings of the 37th International Conference on Machine Learning (ICML)*, 2020.

T. N. Kipf and M. Welling. Semi-supervised classification with graph convolutional networks. *arXiv preprint arXiv:1609.02907*, 2016.

D. Kong, A. Zhang, and Y. Li. Learning persistent community structures in dynamic networks

via topological data analysis. In *Proceedings of the AAAI Conference on Artificial Intelligence*, volume 38, pages 8617–8626, 2024.

S. Kornblith, M. Norouzi, H. Lee, and G. Hinton. Similarity of neural network representations revisited. In *International Conference on Machine Learning*, pages 3519–3529. PMLR, 2019.

J. Leygonie, B. Rieck, M. Moor, and K. Borgwardt. A framework for differentiable topological layer based on persistent homology. *Conference on Neural Information Processing Systems (NeurIPS)*, 2021.

D. Luo, H. You, Y. Guo, and S. Ji. Topology-preserving deep learning for graph representations. *Proceedings of the 29th ACM International Conference on Multimedia*, pages 3734–3742, 2021.

L. McInnes, J. Healy, and J. Melville. Umap: Uniform manifold approximation and projection for dimension reduction. *arXiv preprint arXiv:1802.03426*, 2018.

M. Moor, M. Horn, B. Rieck, and K. Borgwardt. Topological autoencoders. In *International conference on machine learning*, pages 7045–7054. PMLR, 2020.

F. Mujkanovic, S. Geisler, S. Günnemann, and A. Bojchevski. Are defenses for graph neural networks robust? In S. Koyejo, S. Mohamed, A. Agarwal, D. Belgrave, K. Cho, and A. Oh, editors, *Advances in Neural Information Processing Systems*, volume 35, pages 8954–8968. Curran Associates, Inc., 2022.

S. A. Nene, S. K. Nayar, H. Murase, et al. Columbia object image library (coil-20). 1996.

Y. Qin, B. T. Fasy, C. Wenk, and B. Summa. Rapid and precise topological comparison with merge tree neural networks. *arXiv preprint arXiv:2404.05879*, 2024.

M. Raghu, J. Gilmer, J. Yosinski, and J. Sohl-Dickstein. Svcca: Singular vector canonical correlation analysis for deep learning dynamics and interpretability. *arXiv preprint arXiv:1706.05806*, 2017.

A. Sanfeliu and K.-S. Fu. A distance measure between attributed relational graphs for pattern recognition. *IEEE Transactions on Systems, Man, and Cybernetics*, 13(3):353–362, 1983.

O. Shchur, M. Mumme, A. Bojchevski, and S. Günnemann. Pitfalls of graph neural network evaluation. *arXiv preprint arXiv:1811.05868*, 2018.

N. Shervashidze, P. Schweitzer, E. J. van Leeuwen, K. Mehlhorn, and K. M. Borgwardt. Weisfeiler-lehman graph kernels. *J. Mach. Learn. Res.*, 12: 2539–2561, 2011.

J. T. Springenberg, A. Dosovitskiy, T. Brox, and M. Riedmiller. Striving for simplicity: The all convolutional net. *arXiv preprint arXiv:1412.6806*, 2014.

I. Trofimov, D. Cherniavskii, E. Tulchinskii, N. Balabin, E. Burnaev, and S. Barannikov. Learning topology-preserving data representations. In *ICLR 2023 International Conference on Learning Representations*, volume 2023, 2023.

A. Tsitsulin, M. Munkhoeva, D. Mottin, P. Karras, A. Bronstein, I. Oseledets, and E. Mueller. The shape of data: Intrinsic distance for data distributions. In *International Conference on Learning Representations*, 2020.

P. Velickovic, G. Cucurull, A. Casanova, A. Romero, P. Lio, Y. Bengio, et al. Graph attention networks. *stat*, 1050(20):10–48550, 2017.

S. Vishwanathan, N. N. Schraudolph, R. Kondor, and K. M. Borgwardt. Graph kernels. *Journal of Machine Learning Research*, 11(40):1201–1242, 2010.

Y. Wang, H. Huang, C. Rudin, and Y. Shaposhnik. Understanding how dimension reduction tools work: an empirical approach to deciphering t-SNE, UMAP, TriMAP, and PaCMAP for data visualization. *J Mach. Learn. Res*, 22:1–73, 2021.

T. Wen, E. Chen, and Y. Chen. Tensor-view topological graph neural network. In *International Conference on Artificial Intelligence and Statistics*, pages 4330–4338. PMLR, 2024.

H. Xiao, K. Rasul, and R. Vollgraf. Fashion-mnist: a novel image dataset for benchmarking machine learning algorithms. *ArXiv*, abs/1708.07747, 2017. URL `https://api.semanticscholar.org/CorpusID:702279`.

J. Xu, V. Olman, and D. Xu. A fast parallel algorithm for clustering using minimum spanning trees. *IEEE Transactions on Parallel and Distributed Systems*, 1 (3):355–365, 1990.

C. T. Zahn. Graph-theoretical methods for detecting and describing gestalt clusters. *IEEE Transactions on Computers*, C-20(1):68–86, 1971.

A. J. Zomorodian. *Computing and comprehending topology: Persistence and hierarchical Morse complexes. PhD Thesis.* University of Illinois at Urbana-Champaign, 2001.

Checklist

1. For all models and algorithms presented, check if you include:
   (a) A clear description of the mathematical setting, assumptions, algorithm, and/or model. [Yes, Sections 3, 4]
   (b) An analysis of the properties and complexity (time, space, sample size) of any algorithm. [Yes, Sections 3, 4]
   (c) (Optional) Anonymized source code, with specification of all dependencies, including external libraries. [Yes]

2. For any theoretical claim, check if you include:
   (a) Statements of the full set of assumptions of all theoretical results. [Yes, Sections 3, 4, Appendix]
   (b) Complete proofs of all theoretical results. [Yes, Appendix]
   (c) Clear explanations of any assumptions. [Yes, Sections 3, 4]

3. For all figures and tables that present empirical results, check if you include:
   (a) The code, data, and instructions needed to reproduce the main experimental results (either in the supplemental material or as a URL). [Yes]
   (b) All the training details (e.g., data splits, hyperparameters, how they were chosen). [Yes, Appendix]
   (c) A clear definition of the specific measure or statistics and error bars (e.g., with respect to the random seed after running experiments multiple times). [Yes]
   (d) A description of the computing infrastructure used. (e.g., type of GPUs, internal cluster, or cloud provider). [Yes]

4. If you are using existing assets (e.g., code, data, models) or curating/releasing new assets, check if you include:
   (a) Citations of the creator If your work uses existing assets. [Yes]
   (b) The license information of the assets, if applicable. [Yes, Appendix I]
   (c) New assets either in the supplemental material or as a URL, if applicable. [Yes]
   (d) Information about consent from data providers/curators. [Not Applicable]
   (e) Discussion of sensible content if applicable, e.g., personally identifiable information or offensive content. [Not Applicable]

5. If you used crowdsourcing or conducted research with human subjects, check if you include:
   (a) The full text of instructions given to participants and screenshots. [Not Applicable]
   (b) Descriptions of potential participant risks, with links to Institutional Review Board (IRB) approvals if applicable. [Not Applicable]
   (c) The estimated hourly wage paid to participants and the total amount spent on participant compensation. [Not Applicable]

A Proof of the exact sequence

We provide a brief proof of the exactness of the short sequence in Equation 1.

Exactness at $\ker(r_{0,\alpha})$**:** The kernel of inclusion map ι is trivial and coincides with the image of the map from 0.

Exactness at $H_0(A^{\leq\alpha})$**:** The image of ι is $\ker(r_{0,\alpha})$, and the kernel of $r_{0,\alpha}$ is exactly $\ker(r_{0,\alpha})$, satisfying the condition $\mathrm{Im}(\iota) = \ker(r_{0,\alpha})$.

Exactness at $H_0(C^{\leq\alpha})$**:** Since $r_{0,\alpha}$ is surjective onto its image, because each connected component of $C^{\leq\alpha}$ contains at least one vertex from $A^{\leq\alpha}$, and the sequence ends with 0, the exactness condition at $H_0(C^{\leq\alpha})$ is satisfied.

B On some intuition behind RTD-Lite

Point cloud in a metric space can be naturally represented as a full weighted graph (weights are taken as distances between points), so we will talk here only about weighted graphs. Given a finite weighted graph G, consider a sequence of its subgraphs G_α, such that G_α contains all vertices of G and all edges with weights $\leq \alpha$. Let this sequence contain all unique G_α for all meaningful α (it is finite because there is a finite number of different edge weights). With each G_α we associate a simplicial complex, containing a k-dimensional simplex for each $k+1$-element clique in the graph. There is a natural mapping $G_\alpha \to G_\beta$ for $\alpha \leq \beta$, which can be extended to the elements of the simplicial complexes associated with G_α and G_β. Thus, we obtain a *simplicial filtration.*

Essentially, $0-$dimensional topological features are just connected components in the graph, $1-$dimensional are (equivalence classes) of loops. $2-$ and higher ($k-$) dimensional features are just $k-1$-dimensional voids.

Persistence barcode is just another representation for the information on the lifespan of topological features, similar to the Persistence diagrams. A Persistence Barcode is a multiset of intervals $[b_i, d_i]$ corresponding to all topological features where b_i is the threshold at which the topological feature i first appears (birth moment) in the associated filtration and d_i is the threshold at which it disappears (death moment). We can limit to use only information about features from $0-, 1-, \ldots k-$th homology group, thus, obtaining $0-, \ldots$ *dimensional barcodes.*

A topological discrepancy RTD-Lite feature appears at threshold $a = b_e$, when in the union of edges of $A^{\leq e}$ and $B^{\leq e}$, two vertex sets C_1 and C_2 disjoint at smaller thresholds, are joined into one connected component by the edge e from $B^{\leq e}$. This interval is closed at threshold $\alpha = a_{e\prime}$ when the two vertex sets C_1 and C_2 are joined into one connected component by the edge e' in the graph of $A^{\leq\alpha}$.

Essentially, RTD contains in addition features that describe non-trivial cycles appearing in one graph at some scale but not in another.

C Details on the experiment with "clusters"

Figure 7 presents point clouds under comparison: one cluster vs. 2-12 clusters. Figure 6 shows R-Cross-Barcodes and RTD-Lite barcodes for the comparisons which have similarities.

D Additional results for synthetic datasets

Barannikov et al. (2021) carried out experiments with the same datasets "rings" and "clusters" and compared RTD with CKA, SVCCA, IMD. As a quality measure, Barannikov et al. (2021) used Kendall-tau correlation between a metric and a number of rings and clusters respectively. We have calculated the Kendall-tau correlation for RTD-Lite and merged with results of Barannikov et al. (2021).

For "rings", the Kendall-tau rank correlations of the measures with a number of rings are:

RTD-Lite: 0.8, RTD: 0.8, CKA: -0.2, IMD: 0.8, SVCCA: -0.2.

For "clusters", the Kendall-tau rank correlations of the measures with a number of clusters are:

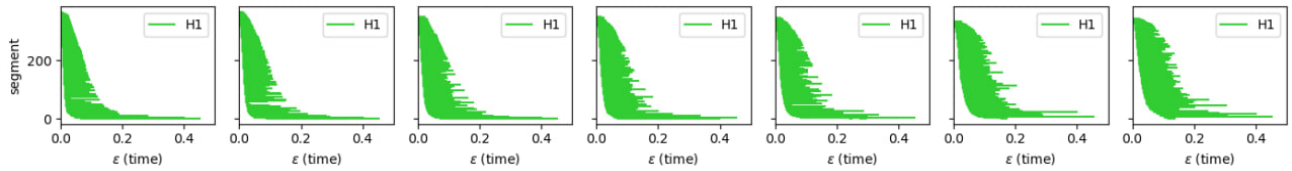

(a) R-Cross-Barcode(A,B).

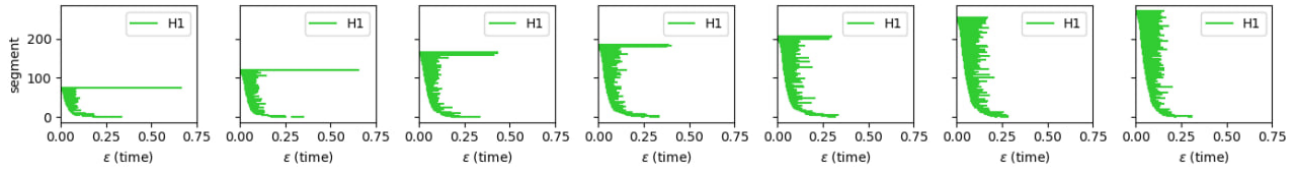

(b) R-Cross-Barcode(B,A).

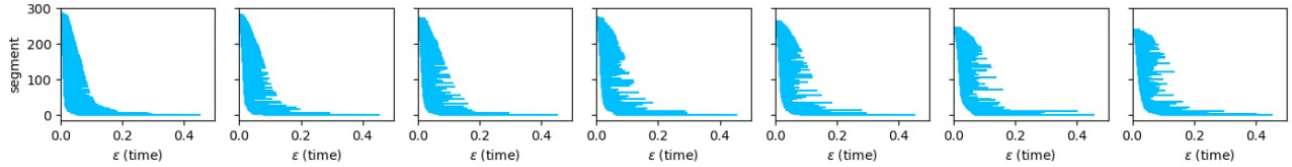

(c) RTD-Lite Barcode(A,B).

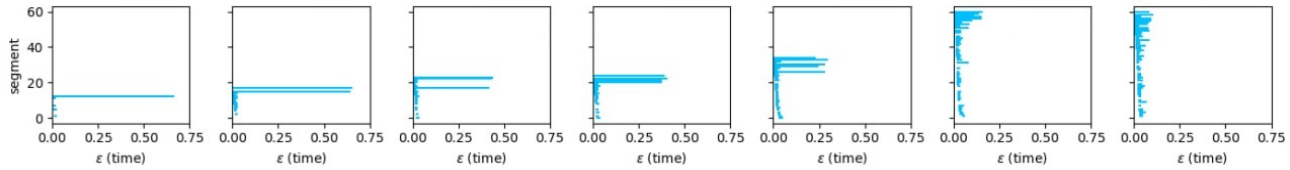

(d) RTD-Lite Barcode(B,A).

Figure 6: Cross-Barcodes for comparison of one cluster vs. 2-12 clusters.

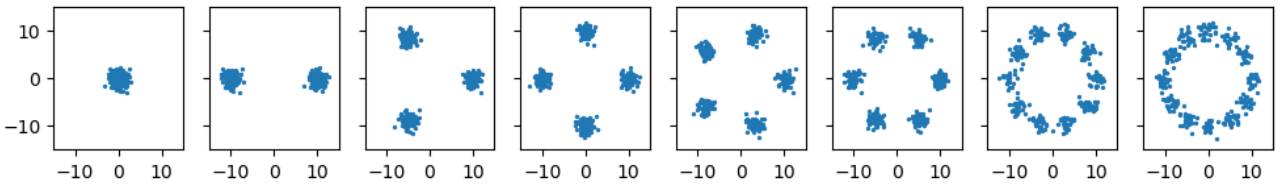

(a) Point clouds used in the "clusters" experiment.

(b) Representations' comparison measures. Ideally, the measure should change monotonically with the increase of topological discrepancy.

Figure 7: Comparison of point clouds via RTD, RTD-Lite, CKA. One cluster is compared to 2-12 clusters.

RTD-Lite: -1.0, RTD: 1.0, CKA: 0.23, IMD: 0.43, SVCCA: 0.14.

In both of these cases, RTD and RTD-Lite show the highest absolute Kendall-tau correlation, meaning that RTD and RTD-Lite correctly capture changes of topological structures. However, for the experiment with "clusters" the dependency between RTD-Lite and the number of clusters is reversed. We would like to emphasize that we do not expect that RTD-Lite will be more sensitive than RTD. Its main benefit is calculation speed.

E Analysis of RTD-Lite for GNN representations

In line with the recent research Ebadulla and Singh (2024), we provide analysis of RTD-Lite for measuring dissimilarity in GNN representations as additional verification for a domain with an inherent complex structure.

E.1 Convergence Analysis

In this experiment, we inspect how layers' representations from a GNN evolve during training as measured by the metrics under analysis: CKA, NSA (Ebadulla and Singh, 2024), RTD, RTD-Lite. We strictly follow the setup from Ebadulla and Singh (2024) and, for each layer, we compare its representations from an intermediate epoch with its representations from the final epoch of training (Figure 8). In general, dissimilarity in representations decreases throughout training as measured by RTD-Lite. Although there are several cases of non-monotonic behaviour in the beginning of training, they are mostly revealed by RTD as well. In Figure 9, we take a closer look at evolution of RTD-Lite vs. RTD throughout training. In most cases, RTD and RTD-Lite are well aligned. Comparison of SAGE layers' representations (Figure 9b) provides the only case when RTD-Lite behaves differently. To some extent, this is natural because RTD-Lite takes into account only 0-dimensional topological features while RTD considers 1-dimensional topological features as well.

E.2 Adversarial attacks analysis

The work Ebadulla and Singh (2024) studies whether dissimilarity between GNNs' representations under adversarial attacks of various intensity is aligned with misclassification rate. We further extend this evaluation and verify whether RTD-Lite is able to capture deterioration of GNNs' classification performance. Following the experimental setup from loc.cit., we apply global evasion and global poisoning adversarial attacks to GCN and robust GNN variants - GCN-SVD (Entezari et al., 2020), ProGNN (Jin et al., 2020), GRAND (Chamberlain et al., 2021) - under various intensity rates. In this setup, adversarial attacks are constructed by introducing perturbations in the range $5\% - 25\%$ into adjacency matrices. For each value of perturbation rate, we compute the dissimilarity between the initial representations and representations under attack. Figure 10 demonstrates that, in general, RTD-lite captures the same tendency as misclassification rate, similar to other metrics. Our

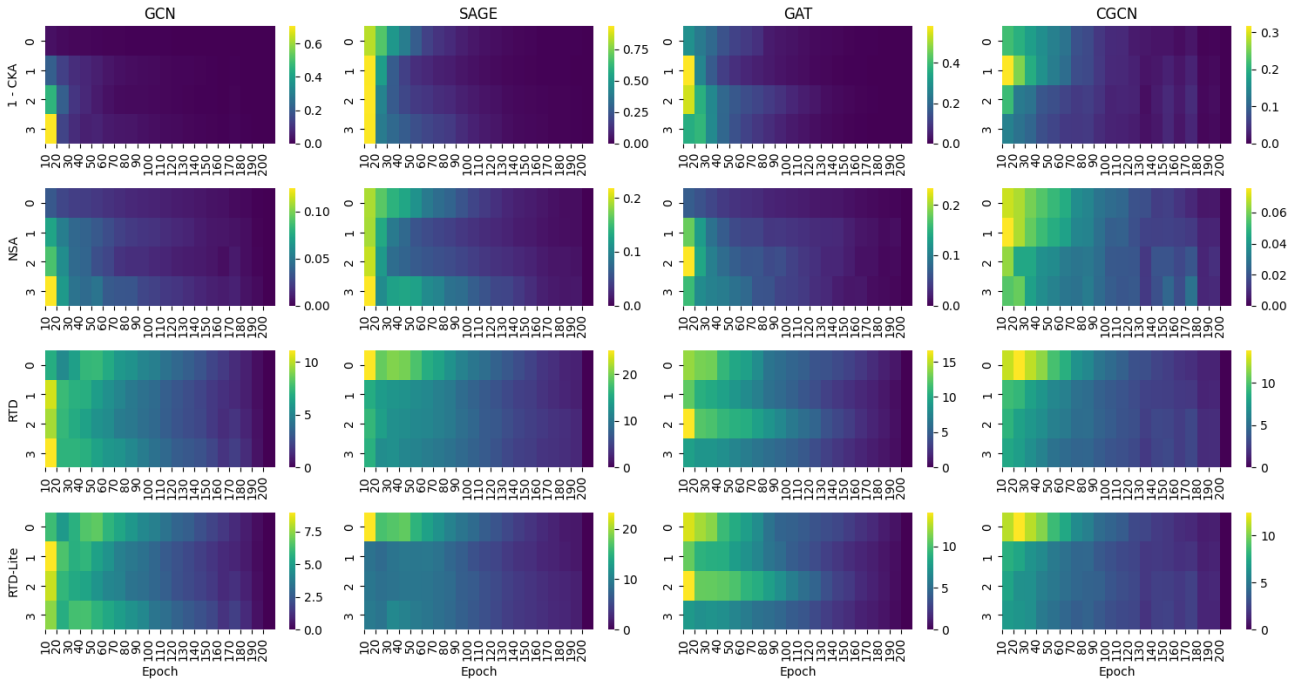

Figure 8: Evolution of dissimilarity in GNNs' representations at an intermediate and final training epochs as measured by CKA, NSA, RTD, RTD-Lite.

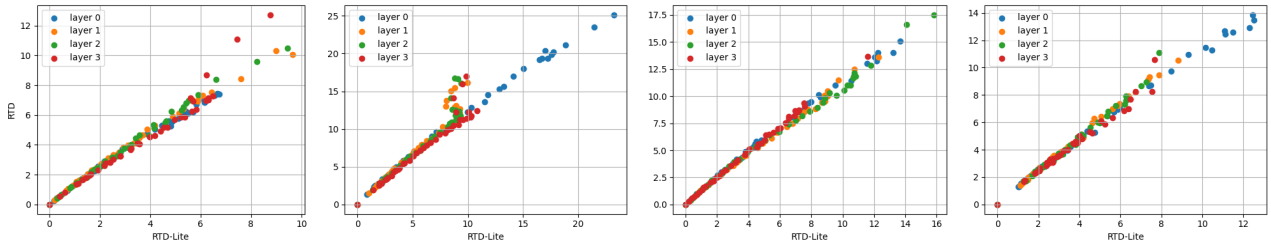

(a) GCN (b) SAGE (c) GAT (d) CGCN

Figure 9: RTD-Lite vs. RTD in measuring dissimilarity between GNN layers' representations at an intermediate and the final training epochs.

experiments also confirm the distinctive behavior of all the representation dissimilarity metrics in the case of evasion attacks for GCN-SVD as was mentioned in Ebadulla and Singh (2024). This effect was attributed to vulnerability in the structure that was also noticed in Mujkanovic et al. (2022). Therefore, RTD-Lite and other metrics are able to reflect potential weaknesses that may be not evident when analysing the misclassification rate solely. In Figures 10k, 10l, we demonstrate that RTD-Lite scores are well aligned with RTD values. Hence, RTD-Lite can be used as an approximation of RTD when its intensive computation is not feasible.

E.3 Additional Evaluation for the experiments from Section 5.1.4

In this section, we provide additional evaluation of CKA, NSA, RTD representation dissimilarity measures for GNN models. Identical to setup from Section 5.1.4, we compare layers' representations from the GNN models (GCN, GraphSAGE, GAT, ClusterGCN) trained with different initialization. Figure 11 provides the mentioned evaluation.

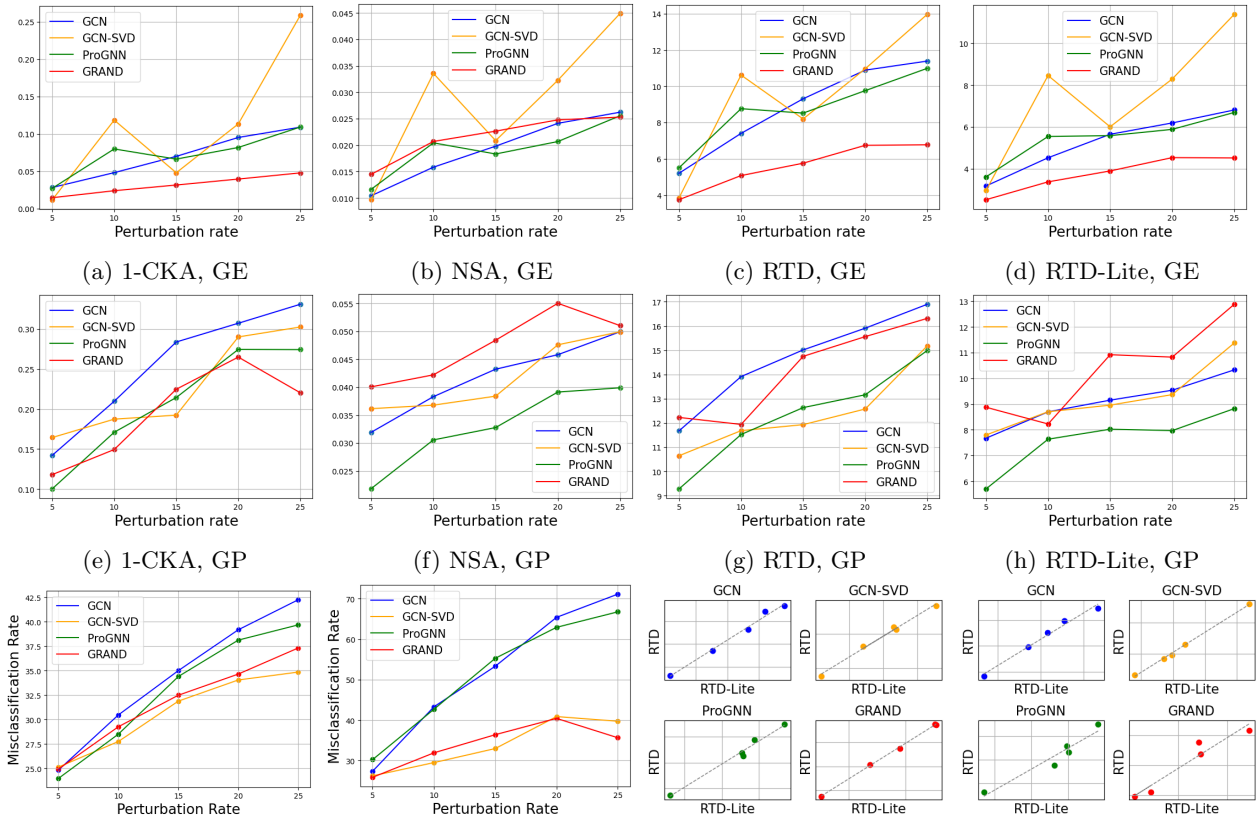

(a) 1-CKA, GE (b) NSA, GE (c) RTD, GE (d) RTD-Lite, GE

(e) 1-CKA, GP (f) NSA, GP (g) RTD, GP (h) RTD-Lite, GP

(i) Misclass. rate, GE (j) Misclass. rate, GP (k) RTD-Lite vs. RTD, GE (l) RTD-Lite vs. RTD, GP

Figure 10: Dissimilarity in GNNs' representations under adversarial attacks of various intensity as measured by CKA, NSA, RTD, RTD-Lite in comparison with misclassification rate: (a - d, i, k) - global evasion attack (GE), (e - h, j, l) - global poisoning attack (GP).

Table 3: GNN test accuracy on Amazon Computer Dataset.

Architecture	Accuracy
GCN	0.8677 ± 0.0004
SAGE	0.9124 ± 0.0007
GAT	0.8920 ± 0.0010
CGCN	0.8689 ± 0.0011

E.4 Training details on GNN experiments

For the experiments on measuring the dissimilarity in representations of GNN, we followed the setup from Ebadulla and Singh (2024). In our experiments with adversarial attacks analysis from Section E.2, we trained GCN, GCN-SVD, ProGNN, GRAND also following the setup from loc.cit. For the experiments from Sections 5.1.4, E.1, we trained GCN, SAGE, GAT, CGCN models with hyperparameters listed in loc.cit., Table 6. Table 3 provides accuracy of our obtained models. We performed the experiments using one Nvidia Titan RTX GPU.

F Experiment details for gradient optimization task

In all reported experiments, for all autoencoder methods (RTD-Lite Autoencoder, RTD-Autoencoder, TopoAE and vanilla Autoencoder) we used the same architecture of deep autoencoder with 3 fully-connected hidden layers having $512, 256,$ and 128 neurons each and ReLU activation function. We used Adam optimizer with learning rate of 0.0001. We did not perform extensive search for optimal value of hyperparameter λ governing the ratio between reconstruction and RTD-Lite loss function components and used $\lambda = 1.0$ (except for COIL-20 dataset, where $\lambda = 5.0$ was used).

For the *Spheres* dataset, training was performed for 100 epochs; RTD-AE was trained for the first 10 epochs using only the reconstruction loss, as suggested in the original paper. The batch size was set to 80.

For the F-MNIST and COIL-20 datasets, training was performed for 250 epochs; RTD-AE was trained for the first 60 epochs using only the reconstruction loss, as suggested in the original paper. The batch size was set to 256.

G Applications at Large Language Models

RTD-Lite can be used to study changes in model internal data representations as caused by the fine-tuning process. For instance, its high performance allows for applications with modern Large Language Models with large context spans. We performed experiments with LLaMA2-7B model, using RTD-Lite to compare topology of intermediate embeddings between base model and its version additionally fine-tuned at processing dialogues.

For this experiment, we gathered two small corpora of English texts and dialogues (1000 entries in each), where texts on average contain 320 ± 52 tokens, dialogues — 181 ± 23 (this translates into number of vertices in corresponding graphs).

Comparing intermediate embeddings We passed each entry through base and chat-tuned models and calculated RTDL between embeddings from each of 32 pairs of corresponding layers. In total, for this experiment we calculated RTDL for $2 * 1,000 * 32 = 64,000$ pairs of graphs originating from Euclidean distances between points in R^{4096}, and on average, processing each took ≈ 0.07 sec for texts and ≈ 0.02 sec for dialogues. On Figure 12 the distributions of RTDL for textual and dialogic data respectfully are plotted. We can see that in the lower half of the model (up to layer 15) difference between RTDL of text and dialogues is small and quite stable, but it begins to grow for upper layers of the model, and from layer 24 upwards it exceeds two standard deviations.

Comparing attention maps We performed similar experiments to compare topology of the corresponding attention maps from base and chat-tuned models. Attention maps can be viewed as weighted directed graphs with vertices corresponding to text tokens. LLaMA2 implements triangular attention (it calculates attention

weights only between a token and all previous), therefore its attention maps can be transformed into undirected graphs without loss of information. Unlike experiments from the previous paragraph, these graphs do not have realization as distance matrices of a point cloud.

LLaMA2-7B has 1,024 attention heads (32 in each layer), thus we calculated RTDL for $2 * 1,000 * 1,024 = 2,048,000$ pairs of graphs.

Figure 13 presents the results.

These observations support the idea that during fine-tuning of a deep model only weights from its later layers are subject to any significant changes. We hope that this approach can be used to better identify border between layers that do and do not require fine-tuning, thus lowering computations needed for model fine-tuning.

H RTD-Lite barcode and the dimensionality of $\ker(r_{0,\alpha})$

Lemma H.1. *Dimensionality of* $\ker(r_{0,\alpha})$ *equals to the number of intervals in RTD-Lite barcode that contains* α.

Proof. By the rank-nullity theorem for the map

$$r_{0,\alpha} : H_0(A^{\leq\alpha}) \to H_0(C^{\leq\alpha}),$$

we obtain:

$$\dim H_0(A^{\leq\alpha}) = \dim\ker(r_{0,\alpha}) + \dim \mathrm{Im}(r_0, \alpha). \tag{2}$$

By construction of the graph C, $r_{0,\alpha}$ is epimorphism, i.e. $\mathrm{Im}(r_0, \alpha) = H_0(C^{\leq\alpha})$. Thus, Equation 2 is equivalent to:

$$\dim\ker(r_{0,\alpha}) = \dim H_0(A^{\leq\alpha}) - \dim H_0(C^{\leq\alpha}). \tag{3}$$

Let us see how $\dim\ker(r_{0,\alpha})$ changes when increasing the value of α via analysing the dimensionalities of homology groups $H_0(A^{\leq\alpha}), H_0(C^{\leq\alpha})$. First, note that for $\alpha = 0$, both $A^{\leq\alpha}$ and $C^{\leq\alpha}$ consist only of n vertices with no edges. Thus, $\dim H_0(A^{\leq\alpha}) = \dim H_0(C^{\leq\alpha}) = n$ and $\dim\ker(r_{0,\alpha}) = 0$. Also, the intersection of the RTD-Lite barcode with $\alpha = 0$ line is empty.

Now let's add to the set of vertices the edges of $C \supseteq A$ one by one in the increasing weight order. Let us increase the value of α from α_1 to the next weight α_2 of an edge from C, $\alpha_2 > \alpha_1$. First, consider the case when the new edge e appends to $A^{\leq\alpha_2}$ compared to $A^{\leq\alpha_1}$. If e connects the two vertices from the same connected component, then $\dim H_0(A^{\leq\alpha_2}) = \dim H_0(A^{\leq\alpha_1})$ and $\dim H_0(C^{\leq\alpha_2}) = \dim H_0(C^{\leq\alpha_1})$ and $\dim\ker(r_{0,\alpha_2}) = \dim\ker(r_{0,\alpha_1})$. If e connects the vertices from the two different connected components, then the two components merge together and $\dim H_0(A^{\leq\alpha_2}) = \dim H_0(A^{\leq\alpha_1}) - 1$. If e corresponds to the vertices from the same connected component in $C^{\leq\alpha_1}$, then $\dim H_0(C^{\leq\alpha_2}) = \dim H_0(C^{\leq\alpha_1})$. In this case, $\dim\ker(r_{0,\alpha_2}) = \dim H_0(A^{\leq\alpha_2}) - \dim H_0(C^{\leq\alpha_2}) = (\dim H_0(A^{\leq\alpha_1}) - 1) - \dim H_0(C^{\leq\alpha_1}) = \dim\ker(r_{0,\alpha_1}) - 1$. If e corresponds to the vertices from different connected components, then $\dim H_0(C^{\leq\alpha_2}) = \dim H_0(C^{\leq\alpha_1}) - 1$ and $\dim\ker(r_{0,\alpha_2}) = \dim H_0(A^{\leq\alpha_2}) - \dim H_0(C^{\leq\alpha_2}) = (\dim H_0(A^{\leq\alpha_1}) - 1) - (\dim H_0(C^{\leq\alpha_1}) - 1) = \dim\ker(r_{0,\alpha_1})$.

Second, consider the case when $A^{\leq\alpha_2} = A^{\leq\alpha_1}$ (and $H_0(A^{\leq\alpha_2}) = H_0(A^{\leq\alpha_1})$) but a new edge e appears in $C^{\leq\alpha_2}$ compared to $C^{\leq\alpha_1}$. If e corresponds to the vertices from the same connected component, then $H_0(C^{\leq\alpha_2}) = H_0(C^{\leq\alpha_1})$ and $\dim\ker(r_{0,\alpha_2}) = \dim\ker(r_{0,\alpha_1})$. If e corresponds to the vertices from different connected components, then $H_0(C^{\leq\alpha_2}) = H_0(C^{\leq\alpha_1}) - 1$ and $\dim\ker(r_{0,\alpha_2}) = \dim H_0(A^{\leq\alpha_2}) - \dim H_0(C^{\leq\alpha_2}) = \dim H_0(A^{\leq\alpha_1}) - (\dim H_0(C^{\leq\alpha_1}) - 1) = \dim\ker(r_{0,\alpha_1}) + 1$.

Thus, there are two cases of a change in $\dim\ker(r_{0,\alpha_1})$:

- $\dim\ker(r_{0,\alpha_2}) = \dim\ker(r_{0,\alpha_1}) - 1$. In this case, the two connected components that were merged in $C^{\leq\alpha}$ for some $\alpha < \alpha_2$ now merge in $A^{\leq\alpha_2}$. This corresponds to closing of the interval (α, α_2) in RTD-Lite barcode.

- $\dim\ker(r_{0,\alpha_2}) = \dim\ker(r_{0,\alpha_1}) + 1$. In this case, there are two connected components that merge in $C^{\leq\alpha_2}$ and not (yet) merge in $A^{\leq\alpha_2}$. This corresponds to opening of the interval (α_2, α) in RTD-Lite barcode for some $\alpha > \alpha_2$.

Therefore, the decrease and increase in $\dim\ker(r_0, \alpha)$ correspond to the closing and opening of intervals in the RTD-Lite barcode. Thus, for each α, $\dim\ker(r_0, \alpha)$ equals the number of intervals in the RTD-Lite barcode that contain α. □

I Licenses of the used assets

Here is the list of licenses for the assets (models and datasets) that we used in this work.

- CIFAR-10, Fashion MNIST (F-MNIST): MIT license
- COIL-20: GNU General Public License v2.0
- MNIST: GNU General Public License v3.0
- LLaMA2-7B: LLAMA 2 COMMUNITY LICENSE AGREEMENT

We do not publish any new models or datasets with this paper.

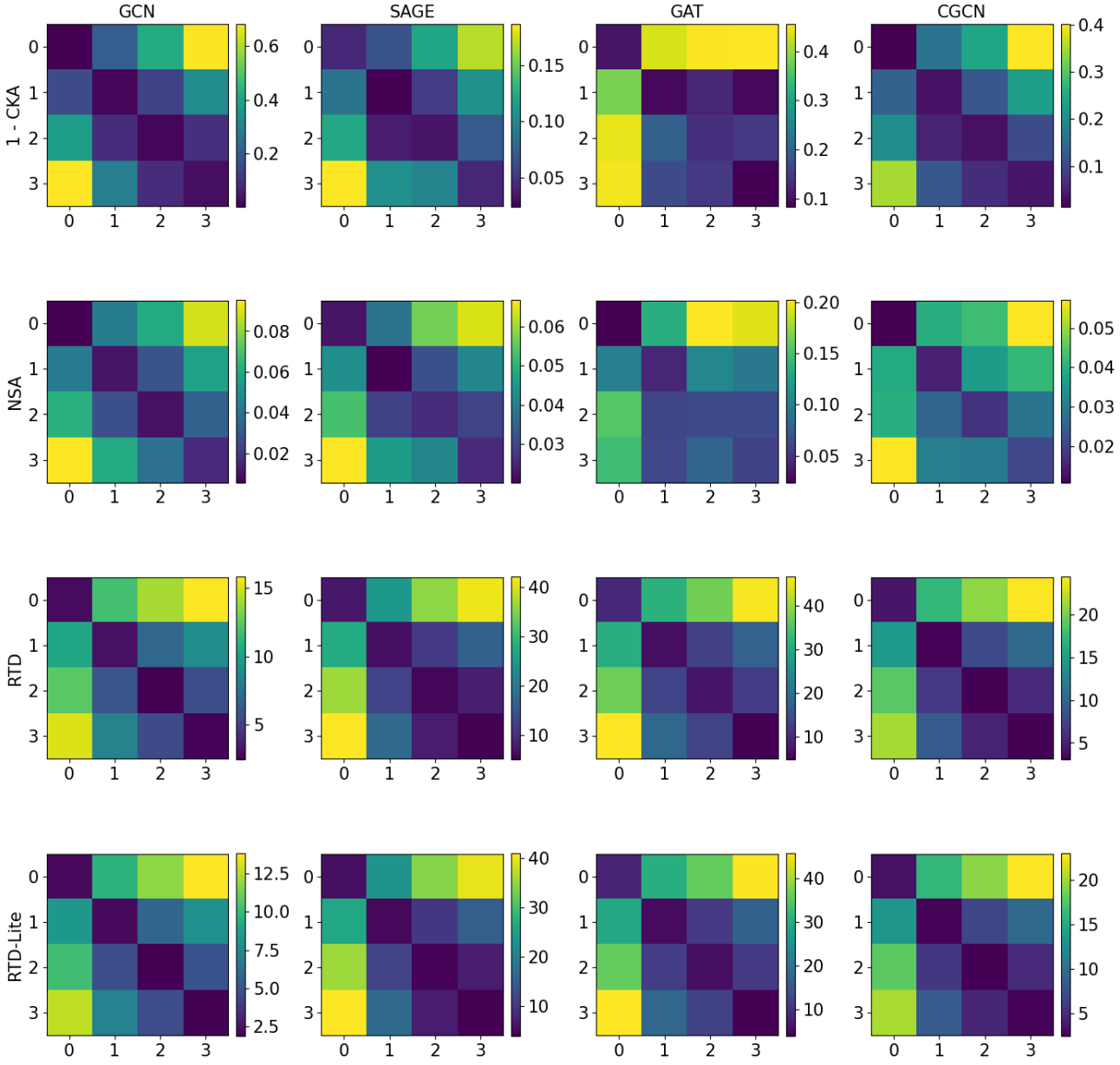

Figure 11: Additional evaluation of CKA, NSA, RTD for the experiment from Section 5.1.4.

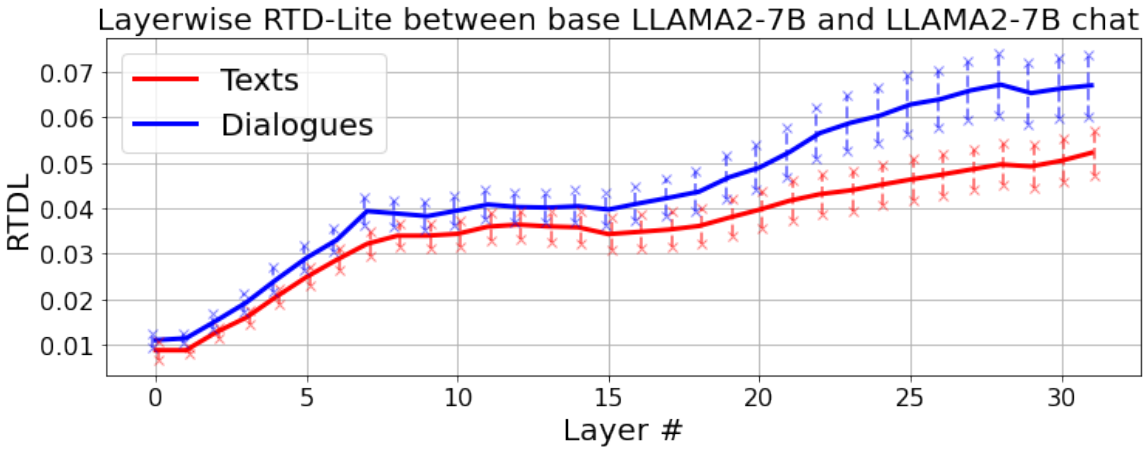

Figure 12: Distributions of RTDL between embeddings of textual and dialogic data from corresponding layers of LLaMA2-7B-base and -chat models. Solid line mark the average, vertical lines – standard deviation.

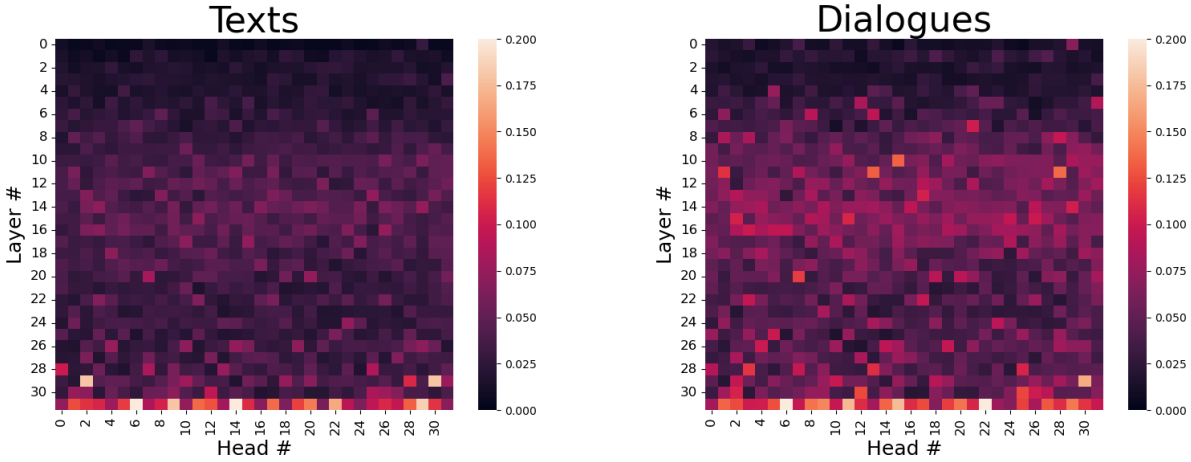

Figure 13: Mean values of RTDL between same heads of LLaMA2-7B-base and -chat-tuned models for same inputs. On the left heatmap for textual data, on the right — for dialogic.